Binding by Random Bursts: A Computational Model of Cognitive Control

Tom Verguts

Abstract

■ A neural synchrony model of cognitive control is proposed. It construes cognitive control as a higher-level action to synchronize lower-level brain areas. Here, a controller prefrontal area (medial frontal cortex) can synchronize two cortical processing areas. The synchrony is achieved by a random theta frequency-locked neural burst sent to both areas. The choice of areas that receive this burst is determined by lateral frontal cortex. As a result of this synchrony, communication between the two areas becomes more efficient. The model is tested on the classical Stroop cognitive control task, and its operation is explored in several simulations. Both reactive and proactive controls are implemented via theta power modulation. Increasing theta power improves behavioral performance; furthermore, via theta–gamma phase–amplitude coupling, theta also increases gamma frequency power and synchrony in posterior processing areas. Thus, the model solves a central computational problem for cognitive control (how to allow rapid communication between arbitrary brain areas), while making rich contact with behavioral and neurophysiological data. ■

INTRODUCTION

Cognitive control is the ability to adapt and respond to novel situations. An important aspect of cognitive control is implementing and obeying essentially arbitrary task rules (i.e., rules for which the stimulus–response mapping is not in long-term memory). How this is mechanistically implemented currently remains unknown. A core computational issue for cognitive control is flexibly (i.e., context-dependent) distinguishing between task-relevant and task-irrelevant processing pathways. To achieve this, theorists have proposed various modulations of neural processing pathways by which cognitive control can be exerted, typically involving some sort of top–down biasing of the relevant processing pathways (Verguts & Notebaert, 2008; Botvinick, Braver, Barch, Carter, & Cohen, 2001; Braver & Cohen, 2000; Desimone & Duncan, 1995).

Computational models implementing top–down biases usually consist of rate code neurons that learn via synaptic changes which processing areas are relevant in which context. In a rate code, the neural firing rate contains the relevant information to be passed on to downstream processing areas. Typically, these models do not exploit the (oscillatory) phase code. Phase coding refers to the use of the phase difference in activation between two neurons or areas (e.g., relative neural firing time; Gray & Singer, 1989) to support information processing. This absence of phase coding in such models is surprising given that oscillatory phase coding is computationally useful to implement rapid binding in several aspects of cognition where flexibility is key, including visual perception (Hummel & Biederman, 1992), visual attention (Jensen, Bonnefond, & VanRullen, 2012), STM (Lisman & Idiart, 1995), and relational reasoning (Hummel & Holyoak, 2003). Relatedly, earlier cognitive control models do not account for the ubiquitous oscillatory brain signatures seen (ever since Hans Berger's initial experimentation in the 1920s) in cognition (Fell & Axmacher, 2011; Engel, Fries, & Singer, 2001), including cognitive control (Cavanagh & Frank, 2014; Pastötter, Dreisbach, & Bäuml, 2013).

To address this issue, an oscillatory model for cognitive control is proposed, thus exploiting the usefulness of oscillations for binding cortical areas. Here, cognitive control emerges from interactions between rate codes, phase codes, and synaptic connections. Phase coding has been proposed to subserve several (related) computational roles, such as binding by synchrony (Gray, König, Engel, & Singer, 1989; Gray & Singer, 1989), feedforward coincidence detection (Fries, 2009), synaptic input gain modulation, communication through coherence (Fries, 2009), and synaptic plasticity (Fell & Axmacher, 2011). Because phase synchrony can change rapidly (Rodriguez et al., 1999; relative to the timescale of cognitive control processes), it is an attractive concept to implement arbitrary task rules, which often require quickly changing interactions between arbitrary cortical processing areas. Because implementing arbitrary task rules is a key aspect of cognitive control, phase synchronization is well suited for implementation of cognitive control.

For this purpose, I combine two earlier principles, namely, noise-induced synchronization (Zhou, Chen, &

Ghent University

Journal of Cognitive Neuroscience 29:6, pp. 1103–1118
doi:10.1162/jocn_a_01117

Aihara, 2005) and communication through coherence (Fries, 2015). To implement noise-induced synchronization, one controller area (here medial frontal cortex [MFC]) sends random bursts that reach other cortical areas. This allows the latter areas to synchronize (via gamma frequency waves, approximately 40 Hz) for cognitive processing. Bursts are phase-locked to the theta (approximately 5 Hz) MFC wave. In the model, the higher the amplitude of this theta wave, the more bursts are sent, and thus the higher its synchronizing impact. The appropriate to-be-bound areas are determined by synaptic connections (currently fixed) in lateral frontal cortex (LFC). To illustrate the principle, consider Figure 1A and B (implemented using Equations 2, 3, and 7 in the Methods section). In Figure 1A, oscillating MFC activation is depicted. In the first time frame (until around 0.3 sec), the MFC wave amplitude is low. In the second time frame (from around 0.3 sec), the MFC wave amplitude increases, which leads to fast successive "spiking" events (bursts; individual events appear in both Figure 1A and B). In Figure 1B, black and red curves represent (gamma frequency) signals of two cortical areas. As a result of the MFC burst, the two areas synchronize. Another visualization appears in Figure 2A: The two red vectors are initially out of phase, but after receiving a "burst" (dashed vectors), they are much closer together (black vectors). Noise-induced synchronization is very robust across different types of oscillators (Nakao, Arai, Nagai, Tsubo, & Kuramoto, 2005).

The second principle is communication through coherence (Fries, 2015). This entails that two areas that are synchronized ("coherent") can communicate more efficiently. Intuitively, the right time for an input area to send information is when the output area is also "open," and this will occur when the two areas are synchronized. The combination of the two principles is called "binding by random bursts" because the random bursts eventually cause the two processing areas to communicate and in that sense bind together.

Cognitive control can operate at slow and fast timescales, corresponding respectively to proactive and reactive control (Braver, 2012). In the model, both are implemented as an increase in MFC theta power, either before stimulus onset (proactive control) or in response

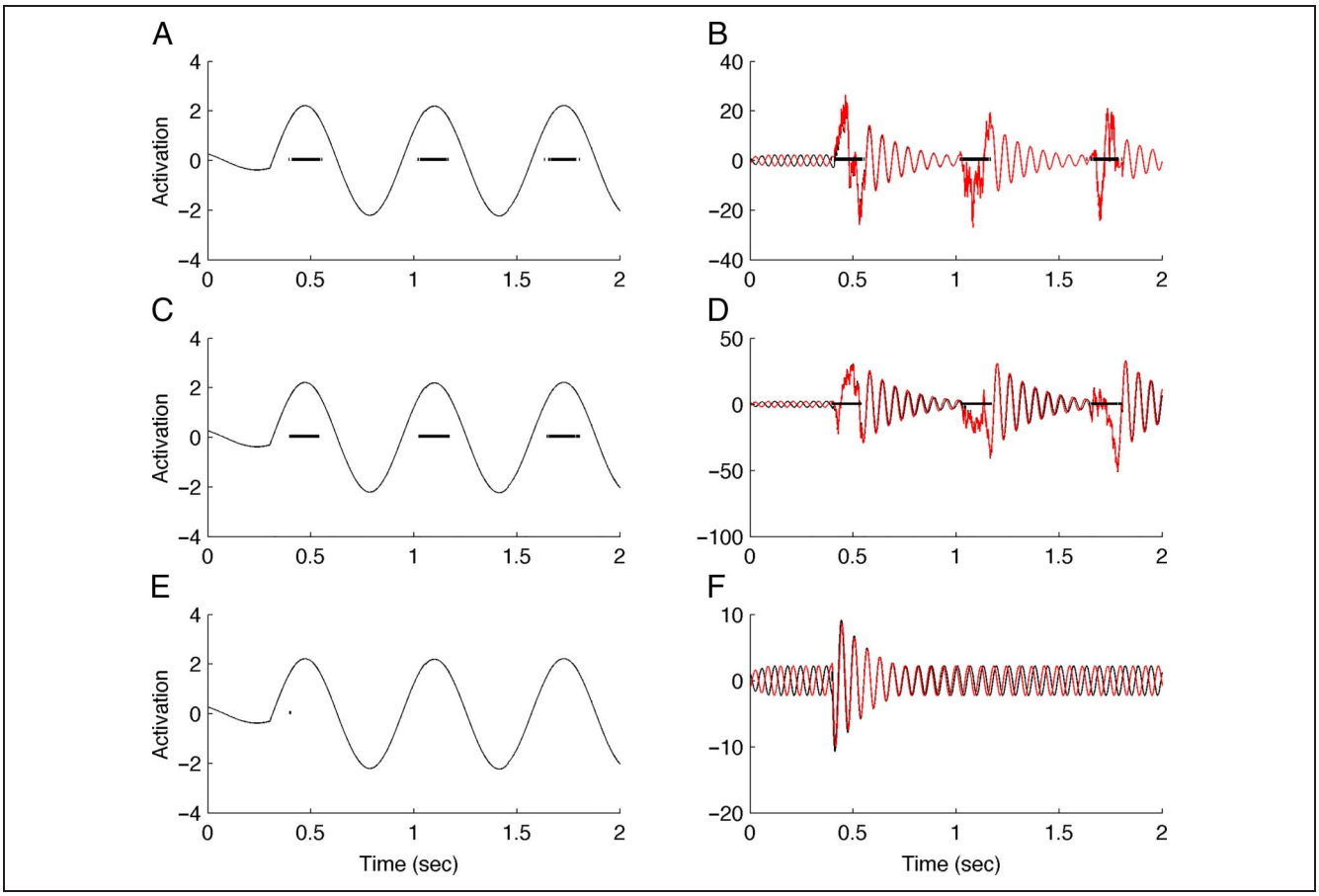

Figure 1. Conceptual illustration of noise-induced synchronization. (A, C, E) Theta wave and bursts. (B) Neurons with the same gamma frequency, receiving bursts shown in A and B. (D) Neurons with slightly offset (2%) gamma frequencies, receiving bursts shown in C and D. Activation waves tend to drift apart relative to one another (i.e., their phase difference increases) but remain synchronized due to the theta bursts. (F) As in D, but only a single burst of theta-locked input is provided (see E). Note that activation gamma waves drift apart, after initial synchronization around time step $t = 0.4$.

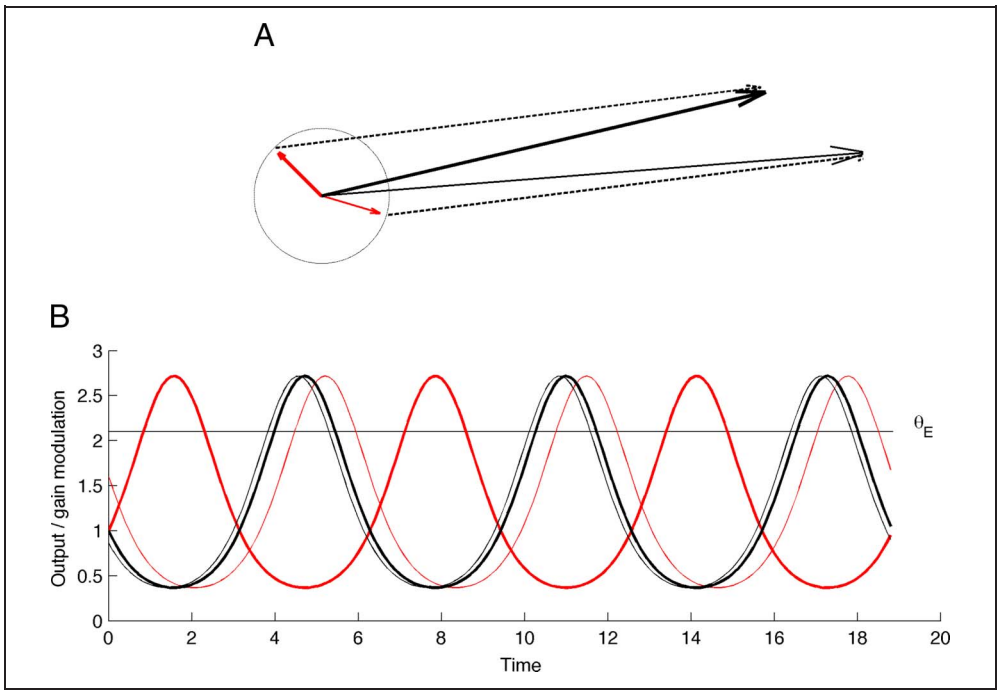

Figure 2. (A) Noise-induced synchronization: Two initially asynchronous vectors (red) receive a "hit" (black, dashed lines) and are synchronous afterwards (black, full lines). (B) Communication through coherence: Two vectors that are synchronous (black) are open at the same time, allowing more efficient communication between them. The y axis represents either output modulation (for sending unit, e.g., thin line waves) or gain modulation (for receiving unit, e.g., thick line waves). Red waves represent cosine of red arrows (corresponding to E-units) after transformation with Equation 6; black curves represent cosine of black arrows (corresponding to E-units), also after transformation with Equation 6. Time is in arbitrary time units in this plot.

to problems encountered during task processing (reactive control). I will explore proactive and reactive control, as well as several other model aspects.

In the simulations, I consider the following empirical effects. First, behaviorally, there is a congruency effect in accuracy and RT, meaning that error probability is higher and RT is slower for incongruent stimuli. Furthermore, with stronger control there are less errors, faster RTs, and smaller congruency effects. This occurs both proactively (e.g., because the reward at stake is higher or because the upcoming task is difficult; Janssens, De Loof, Pourtois, & Verguts, 2016; Vassena et al., 2014; Padmala & Pessoa, 2011) and reactively (e.g., in response to current trial processing difficulty or after an error or incongruent trial; Gratton, Coles, & Donchin, 1992).

A second empirical effect is spectral power in gamma and theta frequency bands. Increased gamma power is associated with better performance in selective attention tasks (Womelsdorf, Fries, Mitra, & Desimone, 2006). Furthermore, theta power in MFC correlates with performance in such tasks, and it increases whenever action is required (Cavanagh & Frank, 2014). A third empirical signature concerns cross-area coupling. A large empirical literature reveals cross-area coupling in specific frequency bands in selective attention and cognitive control (Buschman, Denovellis, Diogo, Bullock, & Miller, 2012; Nigbur, Cohen, Ridderinkhof, & Stürmer, 2012; Womelsdorf, Johnston, Vinck, & Everling, 2010; Gray et al., 1989). In the gamma band, relative phase both within and between cortical areas predicts their interactions (Womelsdorf et al., 2007; Miltner, Braun, Arnold, Witte, & Taub, 1999). A fourth empirical effect is cross-frequency coupling. In several cognitive tasks, gamma amplitude is locked to theta phase (Lisman & Jensen, 2013); furthermore, the theta–gamma coupling strength strongly correlates with behavioral performance (Tort, Komorowski, Manns, Kopell, & Eichenbaum, 2009). In cognitive control tasks, theta–gamma phase–amplitude coupling in MFC has been reported (Voloh, Valiante, Everling, & Womelsdorf, 2015; Canolty et al., 2006). An example is shown in Figure 3A (Voloh et al., 2015): Theta–gamma coupling is stronger after cue onset (presumably, when cognitive control is required), but only on correct trials. Furthermore, the coupling is strongest when theta phase is taken from MFC rather than from other frontal areas. A human subjects example appears in Figure 3B (Canolty et al., 2006),

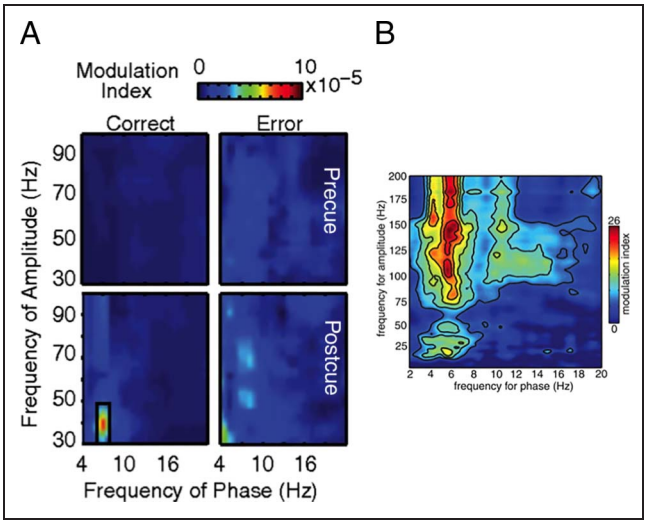

Figure 3. (A) Theta–gamma phase–amplitude coupling data from Voloh et al. (2015). (B) Theta–gamma phase–amplitude coupling data from Canolty et al. (2006).

showing theta–gamma phase–amplitude coupling in several cognitive tasks.

Model Overview

A picture of the model in the context of a standard cognitive control (Stroop) task appears in Figure 4. In this task, subjects must ignore the word and instead name the color of congruent (e.g., RED) or incongruent (e.g., RED) stimuli. The model consists of a processing module, an integrator module, and a control module (Figure 4A). In the processing module, input (in the example, color and word) areas send information to a response area. The integrator module collects (integrates) information from the response area. The control module determines which of the input areas can send its information to the response area.

A key feature of the model is that units (within each area) are cortical columns, consistent with the laminar cortical microcircuit structure of neocortex (Schroeder & Lakatos, 2009; Douglas, Martin, & Whitteridge, 1989). The cortical column is here simplified as a triplet of neurons (see Figure 4B). Each column contains a rate code neuron. Rate code neurons receive, process, and transmit information (e.g., corresponding to neurons in granular layer 4). Each column also contains two phase code neurons, one excitatory (E) and one inhibitory (I) (e.g., corresponding to neurons in infra- and supragranular layers; Giraud & Poeppel, 2012; Lakatos et al., 2009; Schroeder & Lakatos, 2009). Phase code neurons organize the processing of rate code neurons so that information is transmitted to the appropriate processing areas. In particular, because of between-area synchronization of phase code neurons, the relevant input area can send information more efficiently to the response area, even when the irrelevant (word-reading) pathway is synaptically stronger than the relevant (color-reading) pathway. Thus, the model implements communication through coherence (Fries, 2015). This coherence (synchrony) is due to random theta-locked bursts from MFC (Figure 1A, B). Only color and response areas are synchronized because they are tagged by LFC as eligible for MFC bursts. Hence, none of the modules (or areas within modules) has a particularly sophisticated job, but their joint effort implements cognitive control. I next explain the separate modules in detail, followed by a demonstration on how the model works by manipulating several of its parameters across seven simulations.

METHODS

Processing Module

The processing module consists of two input areas (two units each, see Figure 4A) and one response area (also two units). In the Stroop task considered here, one input area represents color and the other (irrelevant) input area represents verbal input. Obviously, the framework can be generalized to different tasks (e.g., Simon task) and task configurations.

In each neural triplet (Figure 4B), phase code neurons appear in excitatory–inhibitory pairs of neurons (E_i, I_i). Rate code units are denoted by x_i. Using G for any of the variables (E, I, x), all neurons obey the update rule:

$$G_i(t + \mathrm{d}t) = G_i(t) + \mathrm{d}t\mathrm{d}G_i(t) \quad (1)$$

where $G \in \{E, I, x\}$, $\mathrm{d}t$ is a small time constant (in sec, $\mathrm{d}t = 3 \times 10^{-4}$), and $\mathrm{d}G_i(t)$ is the change in the

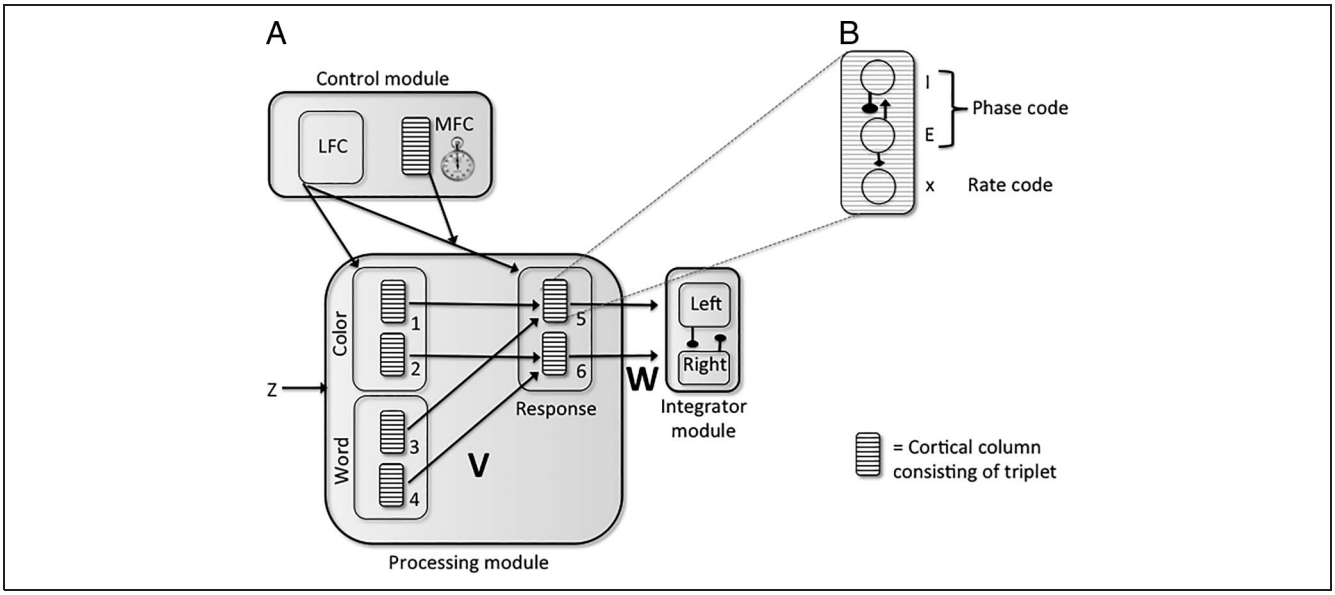

Figure 4. Model sketch. (A) Control module (LFC and MFC), processing module (with Color the task-relevant area), and integrator module. (B) A cortical column is the basic processing unit. It consists of a triplet of neurons. Each unit in the processing module consists of such a triplet (illustrated for one response area unit).

corresponding variable at time step t. Each neuron type is thus characterized by its update $dG_i(t)$. Phase code (E, I) and rate code (x) neurons are now discussed in detail.

Phase Code Neurons

For excitatory neurons E_i, the update ($dG_i(t)$) in Equation 1 becomes

$$dE_i(t) = -CI_i(t) - DJ(r > r_{\min})E_i(t) + B_i(t) \qquad (2)$$

and for inhibitory neurons

$$dI_i(t) = CE_i(t) - DJ(r > r_{\min})I_i(t) \qquad (3)$$

The two neurons are thus coupled via parameter C. As a result, the two neurons will oscillate with frequency $C/(2\pi)$ (Onslow, Jones, & Bogacz, 2014; Li & Hopfield, 1989). Values for parameter C were chosen such that the gamma frequencies were sampled from a distribution with mean 40 (Hz) and standard deviation of 1. Furthermore, within each model replication m ($m = 1, \ldots, nrep$), the gamma frequencies of individual (E, I) neuron pairs varied around a mean value σ_m with a standard deviation σ_γ. Parameter σ_γ expresses to what extent neurons in a given model replication have the same gamma frequency. For example, when $\sigma_\gamma = 0$, all E and I neurons in a given model replication have the same gamma frequency, but different model replications might still have a different gamma frequency. Hence, σ_γ measures how strongly gamma frequencies differ in one single model replication m.

The radius $r = E^2 + I^2$ of a pair of neurons (E, I) is "attracted" toward a radius $r_{\min} = 1$. Biologically, dependence of E and I units on the radius r can be implemented by a common pool of units that E and I units project to, as in earlier implementations of normalization (Wong & Wang, 2006). Here, it is simply implemented by the term $DJ(r > r_{\min})E_i(t)$ (Equation 2) or $DJ(r > r_{\min})I_i(t)$ (Equation 3), where $J(\cdot)$ is an indicator function, which is 1 if its argument is true and 0 otherwise and $D = 0.01$. The excitatory neurons are additionally subject to a burst term $B_i(t)$,

$$B_i(t) = MFC(t)LFC_iU(t) \qquad (4)$$

Hence, the MFC (signal $MFC(t)$) and LFC (top–down signal LFC_i, constant in a trial) together determine the burst signal ($B_i(t)$) to processing module unit i (see full explanation below, Control module section). $U(t)$ is a standard Gaussian variable (sampled at every time step t) The correlation between $U(t)$ values arriving in two different areas is called "burst correlation" in the Results section.

Rate Code Neurons

The x neurons obey

$$\tau dx_i(t) = -x_i(t) + (\mathbf{Vx}(t) + Z_i(t)) \cdot f(E_i(t)) \qquad (5)$$

The parameter τ (=1/600) is a time constant. Each x_i neuron is subject to decay $-x_i(t)$. Each x_i neuron receives internal stimulation (i.e., from the processing module) as implemented in the matrix $\mathbf{V}$. The exact connectivity is illustrated in Figure 4A; units i and j unconnected by arrows have $\mathbf{V}_{ij} = 0$; units connected in the color (task-relevant) pathway have $\mathbf{V}_{ij} = 1$; units connected in the word (task-irrelevant) pathway have $\mathbf{V}_{ij} = 1.1$. This 10% increase in the irrelevant pathway implements the idea that word processing is more automatic than color processing (Cohen, Dunbar, & McClelland, 1990).

Input x_i neurons (in Color and Word areas in the example) additionally receive external stimulation ($Z_i(t)$; see Figure 4). The external stimulation depends on which stimulus is shown on that trial ($Z = 1$ for a neuron's preferred stimulus and $Z = 0$ otherwise). External and internal stimulation are added and multiplied by a sigmoid-increasing function $f(E_i)$ of its corresponding phase unit E_i (see Equation 5). This function $f(E_i)$ implements the concept that the E neurons exert a general excitatory (multiplicative) input to the x units, but only if the excitatory E neuron is sufficiently active. In particular,

$$f(E_i(t)) = \frac{1}{1 + \exp(-5(E_i(t) - \theta_E))} \qquad (6)$$

Functionally, this transforms a harmonic oscillation (implied by Equations 2 and 3) into a nonharmonic oscillation (Fries, 2015), effectively only allowing information transmission between processing areas if E is above the phase threshold θ_E (see also Figure 2B). Alternatively, one could let the inhibitory (rather than excitatory) neurons influence the x neurons, which would phase-shift all processes.

Integrator Module

Consistent with general update Equation 1, updates in the integrator module are given by

$$dy_i(t) = \mathbf{Wx}(t) + \mathbf{W}_{\text{inh}}\mathbf{y}(t) + \sigma_{\text{noise}}N(t)$$

with coupling matrix $\mathbf{W}$ as specified in Figure 4A; unconnected neurons in Figure 4A have $\mathbf{W}_{ij} = 0$ and connected ones have $\mathbf{W}_{ij} = 15$. Finally, matrix $\mathbf{W}_{\text{inh}}$ implements lateral inhibition between the y neurons; diagonal elements are zero, and off-diagonal elements are -0.15. This set of equations implements a competitive accumulator model (Usher & McClelland, 2001). The network gives a response when one of the two y neurons reaches a fixed response threshold of $\theta_y = 2$, at which point both RT and accuracy can be recorded. Finally, a noise variable

$\sigma_{Noise}N(t)$ is added with $N(t)$ a standard-normal Gaussian and $\sigma_{Noise} = 30$.

Control Module

The control module controls information transfer in the processing module. It consists of two areas, MFC and LFC.

Medial Frontal Cortex

The MFC consists of a single column (triplet). One part is an *E-I* pair like in the processing module ($E_{MFC}(t)$ and $I_{MFC}(t)$; Equations 2 and 3), but with theta frequency and $D_{MFC} = 0$. To show model robustness, theta frequencies were not strictly fixed at 5 Hz; instead C values were sampled such that theta frequencies followed a distribution with mean of 5 and standard deviation of 1 (note, frequency = $C/(2\pi)$). The rate code MFC neuron has activation

$$MFC(t) = Be\left(\frac{1}{1+\exp(-5(E_{MFC}(t)-\theta_{MFC}))}\right) \quad (7)$$

Here $Be(p)$ is a Bernoulli process, which is 1 with probability p; as a result it will typically be 1 if the $E_{MFC}(t)$ wave is near its top (Voloh et al., 2015) and its amplitude is sufficiently strong.

One can think of the pair ($E_{MFC}(t)$, $I_{MFC}(t)$) as a stopwatch rotating at theta frequency that sends random bursts to the processing module (via $MFC(t)$) but only in a specific time window (e.g., around 12 o'clock; see Figures 2A and 4A). The size of the control signal (size of the stopwatch) can be manipulated both proactively and reactively. Both proactive and reactive control (σ_{Pro} and σ_{Re}, respectively) are implemented as multiplicative boosts to the MFC stopwatch ($E_{MFC}(t)$, $I_{MFC}(t)$). In particular, at cue onset, the vector ($E_{MFC}(t)$, $I_{MFC}(t)$) becomes $\sigma_{Pro} \times (E_{MFC}(t), I_{MFC}(t))$, and when conflict is detected, the vector ($E_{MFC}(t)$, $I_{MFC}(t)$) becomes $\sigma_{Re} \times (E_{MFC}(t), I_{MFC}(t))$. Default values were $\sigma_{Pro} = \sigma_{Re} = 1$ (Table 1).

Lateral Frontal Cortex

LFC is modeled implicitly, in the sense that the binary variables LFC_i index whether LFC sends a top–down input to processing module unit i. One can think of LFC_i as an eligibility signal; only processing module units that receive such a signal will receive bursts from MFC (see Equation 4). If $LFC_i = 0$, then processing module unit i is not eligible to receive such bursts. In that case, unit i cannot phase-lock to the response area. As a result, its information will arrive inefficiently to the integrator module. The variables LFC_i have no time index t because they are constant across the trial timescale. They represent connections from LFC to input (Color, Word) and response area units. Although fixed in the current simulations, they might be learned via rapid Hebbian learning during instructions, as proposed by several computational models of instruction following (Huang, Hazy, Herd, & O'Reilly, 2013; Ramamoorthy & Verguts, 2012; Doll, Jacobs, Sanfey, & Frank, 2009).

Table 1. Default Parameter Values

Parameter	σ_{Pro}	σ_{Re}	*Burst Correlation*	σ_γ	θ_{MFC}	θ_E	θ_y
Value	1	1	1	0	1.5	0.6	2

Simulations

All default parameters are shown in Table 1. Except when a parameter was systematically manipulated (e.g., σ_{Pro} in the Proactive control simulation), these settings were used in all simulations. Congruent and incongruent stimuli were presented 50% each. Each trial started with a rest period of 0.4 sec (corresponding to a rest period before actual stimulation). Then oscillations in E and I neurons were "switched on" (corresponding to fixation cross onset in a typical experiment), together with proactive control (boost σ_{Pro} to E and I neurons). 0.1 sec later, also the external stimulation (i.e., variables $Z_i(t)$) was presented. RT occurred on average around 800 msec (measured from trial onset), but for the purpose of the time–frequency plots, oscillations were only switched off at 2.4 sec. Each trial ended at 3 sec. I ran $nrep = 40$ replications for each parameter setting, each consisting of 30 trials.

Reactive control requires operationalization of when there is a need for cognitive control. For convenience, response conflict was used, defined as $y_1(t) \times y_2(t)$, as in prominent earlier models (Botvinick et al., 2001). Signals highly correlated with response conflict such as prediction error (Alexander & Brown, 2011; Silvetti, Seurinck, & Verguts, 2011) are expected to lead to similar results. When response conflict crosses a conflict threshold (of 1.5), the ($E_{MFC}(t)$, $I_{MFC}(t)$) pair is multiplied by reactive control parameter σ_{Re}.

Data Analysis

Time–frequency results are plotted for illustrative purposes for two of the proactive control simulations. Gaussian noise ($SD = 4$) was added to each unit before time–frequency analysis, implementing the idea that local field potential (LFP)/MEG/EEG measures only a noisy version of the neurophysiological signal. Time–frequency analyses were performed using code from (Cohen, 2014b).

Time–frequency signal decomposition was performed by convolving the signal (e.g., for an E neuron) by complex Morlet wavelets $e^{i2\pi tf}e^{-t^2/(2\sigma^2)}$, where $i^2 = -1$, t is time, f is frequency of the wavelet, and σ is the "width" of the wavelet, and the magnitude of the complex signal was the power at time t and frequency f. I set $\sigma = 3/(4f)$

so there were approximately three waves in each wavelet (σ as defined here is unrelated to σ_{Re}, σ_{Pro}). Power (squared amplitude) and phase were extracted at each frequency and time point. Afterwards, power at each frequency f was transformed to a decibel scale as $10 \times \log(\text{power}(t))/\log(\text{power}(\text{baseline}))$, where power (baseline) is the mean power in the baseline interval from 0 to 0.1 sec.

Synchrony was calculated using the phase-locking value (Lachaux, Rodriguez, Martinerie, & Varela, 1999), at time step t, frequency f, and signal pairs (j, k),

$$PLV = \frac{1}{N}\left|\sum_{n=1}^{N} \exp\left(i\left(\theta_j(f,n,t) - \theta_k(f,n,t)\right)\right)\right|$$

where $n = 1, \ldots, N$ ranges across the $N = 30$ trials and $\theta_j(f, n, t)$ is the extracted phase for signal j, at frequency f, trial n, and time step t. For plotting mean power and synchrony (Figure 5), relevant indices were calculated from time 0.5 sec until trial end, in a narrow band (4 Hz) around the relevant frequencies. The range of the confidence bars equals ±2 standard errors, calculated as the standard deviation across simulations divided by $\sqrt{nrep}$.

The phase–amplitude modulation index (Canolty et al., 2006) was calculated as

$$MI = \frac{1}{N}\left|\sum_{n=1}^{N} A_j(f_1,n,t)\exp(i\theta_k(f_2,n,t))\right|$$

where $A_j(f, n, t)$ is the amplitude in signal j, at frequency f, trial n, and time step t. Frequencies f_1 and f_2 are typically fast and slow frequencies, respectively. The modulation index was not normalized because all values are compared across control parameters, allowing direct across-condition comparison of the modulation indices.

RESULTS

Simulation 1: Proactive Control

Proactive control entails control before task stimulus onset. I implement it by varying the initial MFC signal amplitude at trial onset (in excitatory [E_{MFC}] and inhibitory [I_{MFC}] neurons). These initial values were sampled from a mean-centered normal distribution with standard deviation of 1, but multiplied by σ_{Pro}. If σ_{Pro} is large, then

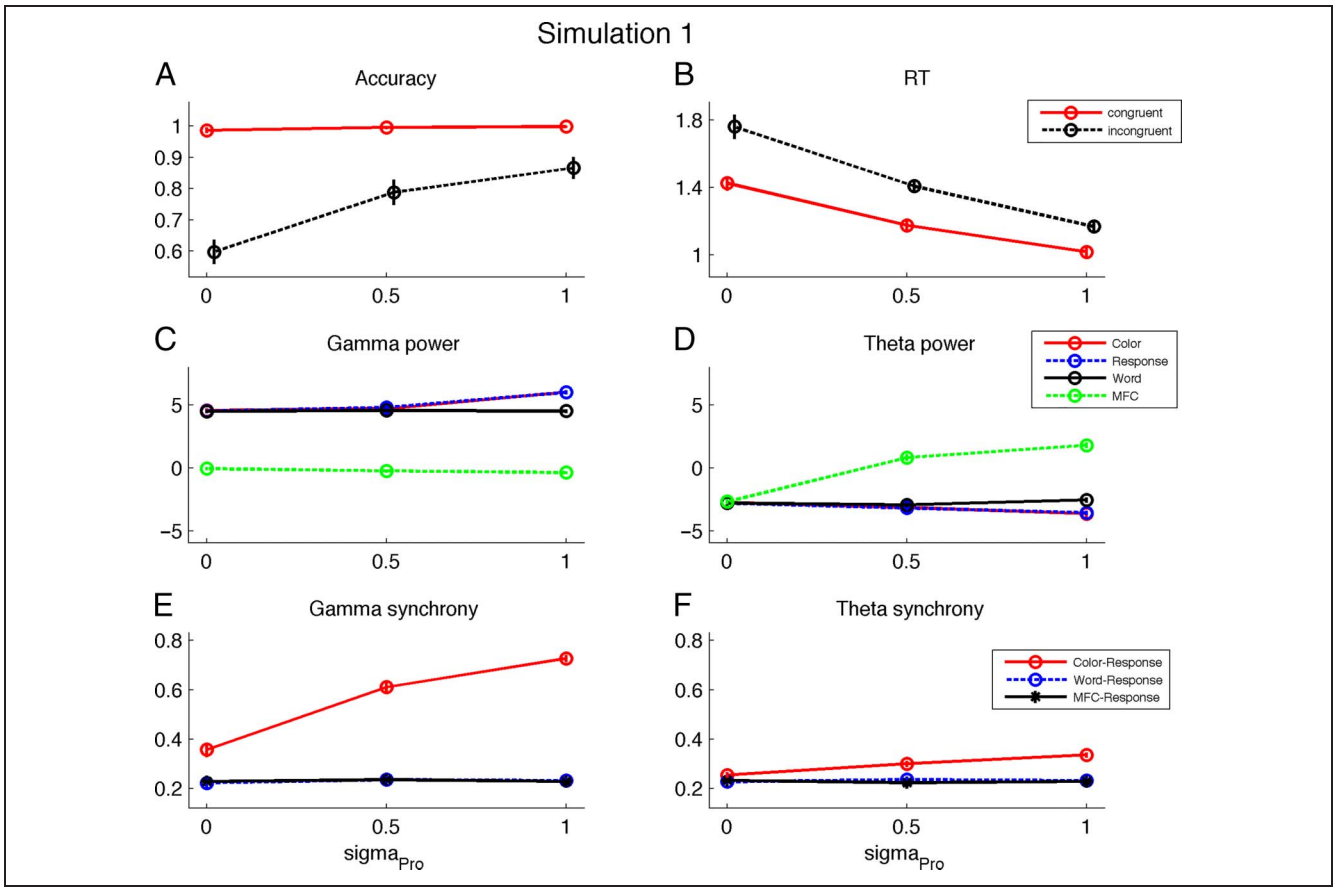

Figure 5. Average behavioral and spectral data from the proactive control simulation (Simulation 1). (A) Mean accuracy for each level of σ_{Pro}. (B) Mean RT for each level of σ_{Pro}. (C) Mean gamma power for each level of σ_{Pro}. (D) Mean theta power for each level of σ_{Pro}. (E) Mean gamma band synchrony for each level of σ_{Pro}. (F) Mean theta band synchrony for each level of σ_{Pro}.

the radius of the circle where the values $(E_{MFC}(t), I_{MFC}(t))$ oscillate on, will tend to be large (see Methods), which increases control. Proactive control was manipulated as $\sigma_{Pro} = 0$, 0.5, or 1.

Selected spectral plots are shown for illustration, but averages (accuracy, RT, power, synchrony, and phase–amplitude coupling) are calculated across all replications (40 replications per parameter value, see Methods). Because this is a "between-subject" design, overlap (or not) between means and confidence bars determines statistical significance (Loftus & Masson, 1994).

Accuracy is consistently high if sufficient proactive control is exerted, even though the irrelevant word-reading pathway (i.e., Word to response area) is synaptically stronger (Figure 5A). Note that LFC simply indicates which input dimension is relevant; it does not specify the required response for a given color. The latter information is encoded in the weight matrix **V**. The LFC only indicates that all units in a given input or response dimension are eligible for synchronization. In that sense, the LFC contains a hierarchically higher set of weights than encoded in **V**. Furthermore, increasing power (control amplitude or σ_{Pro}) improves both accuracy (Figure 5A) and RT (Figure 5B).

Figure 6 illustrates binding by random bursts in the model. Figure 6A shows activation during one trial for four phase code excitatory (*E*) neurons: from (task-relevant) Color input, (task-irrelevant) Word input, response area, and MFC. Activation of *I* neurons is not plotted, but each *I* neuron is typically phase-shifted $\pi/2$ relative to an *E* neuron (Li & Hopfield, 1989). At trial onset, all signals are out of phase (see also zoom-in in Figure 6B). The MFC wave sends random bursts (first burst around 0.75 sec); as a result of this burst, the Color and response area neurons synchronize (see also zoom-in in Figure 6C). Intuitively, if two asynchronous runners are kicked outside a stadium in the same direction, they will be closer together after they return into the stadium (cf. Figure 2A). After a few kicks, they become fully synchronized. In Figure 6, the red curve represents a neuron from the irrelevant (word) input area. Because this neuron does not receive the burst, it remains desynchronized from the green response wave.

Figure 7 shows time–frequency plots for Simulation 1. Figure 7A–B plots the time–frequency spectrum in a color unit *E* neuron for the two extreme levels of control amplitude ($\sigma_{Pro} = 0$ and 1). In this color neuron, gamma power increases with stronger control signals. Figure 7C–D plots the same power values in a word unit *E* neuron. It also has gamma power, but less (particularly in the high-control case $\sigma_{Pro} = 1$), because it does not receive the MFC bursts.

Figure 7E–H shows synchronization (phase-locking value; see Methods) between selected neurons. Figure 7E–F represents synchrony between a color and response neuron, for low ($\sigma_{Pro} = 0$) and high ($\sigma_{Pro} = 0.1$) proactive

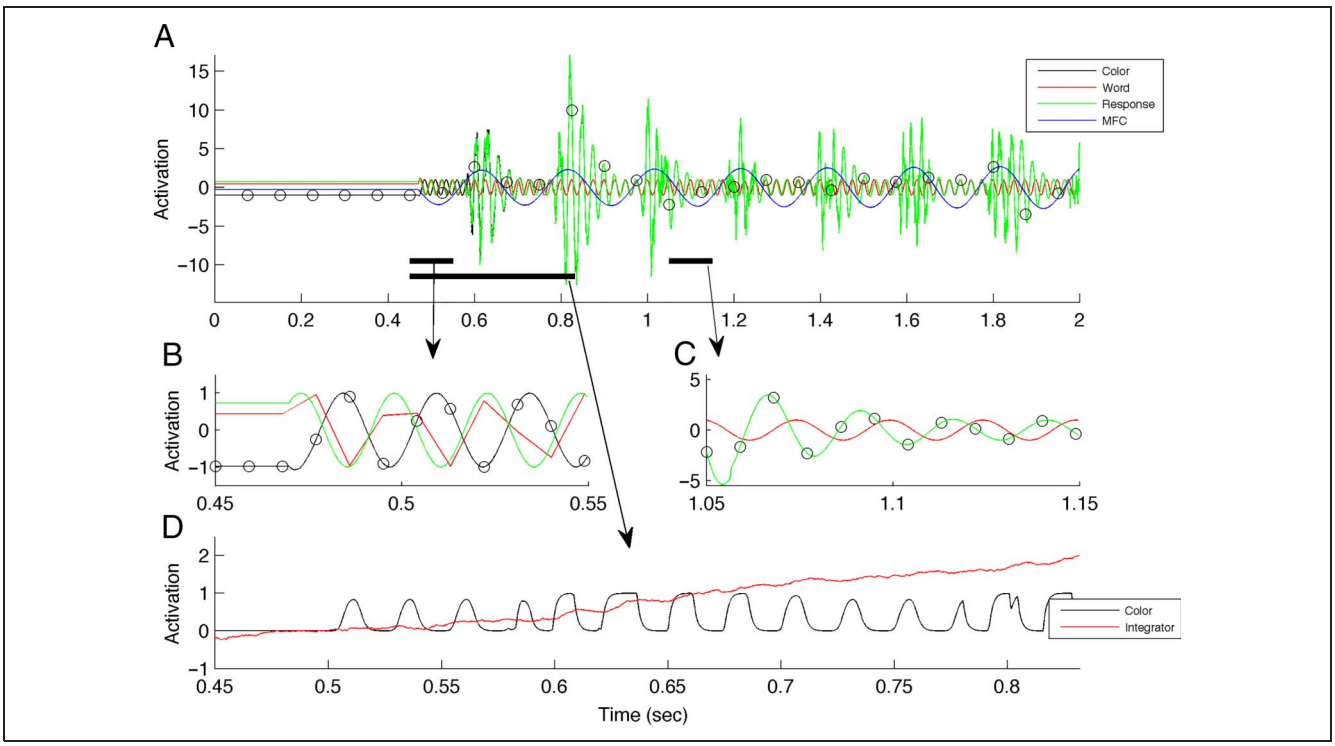

Figure 6. Illustration of key model principles. (A) Time represents 2.5 sec of simulation. Note that color and response amplitude are locked to MFC E-unit (excitatory neuron) phase (blue curve). This binds the appropriate (color) input and response units together. Note also that green and black curves completely overlap after the first burst event. Black dots are added to the black curve to show its trajectory. (B–C) Two zoom-ins of the total time plot (before and after first burst, respectively); intervals correspond to the two short black bars in A (first and second short black bar in B and C, respectively). (D) Evolution of a color and integrator neuron until response is emitted (when the integrator neuron hits the response threshold θ_y of 2; time interval indicated by the long black bar in A).

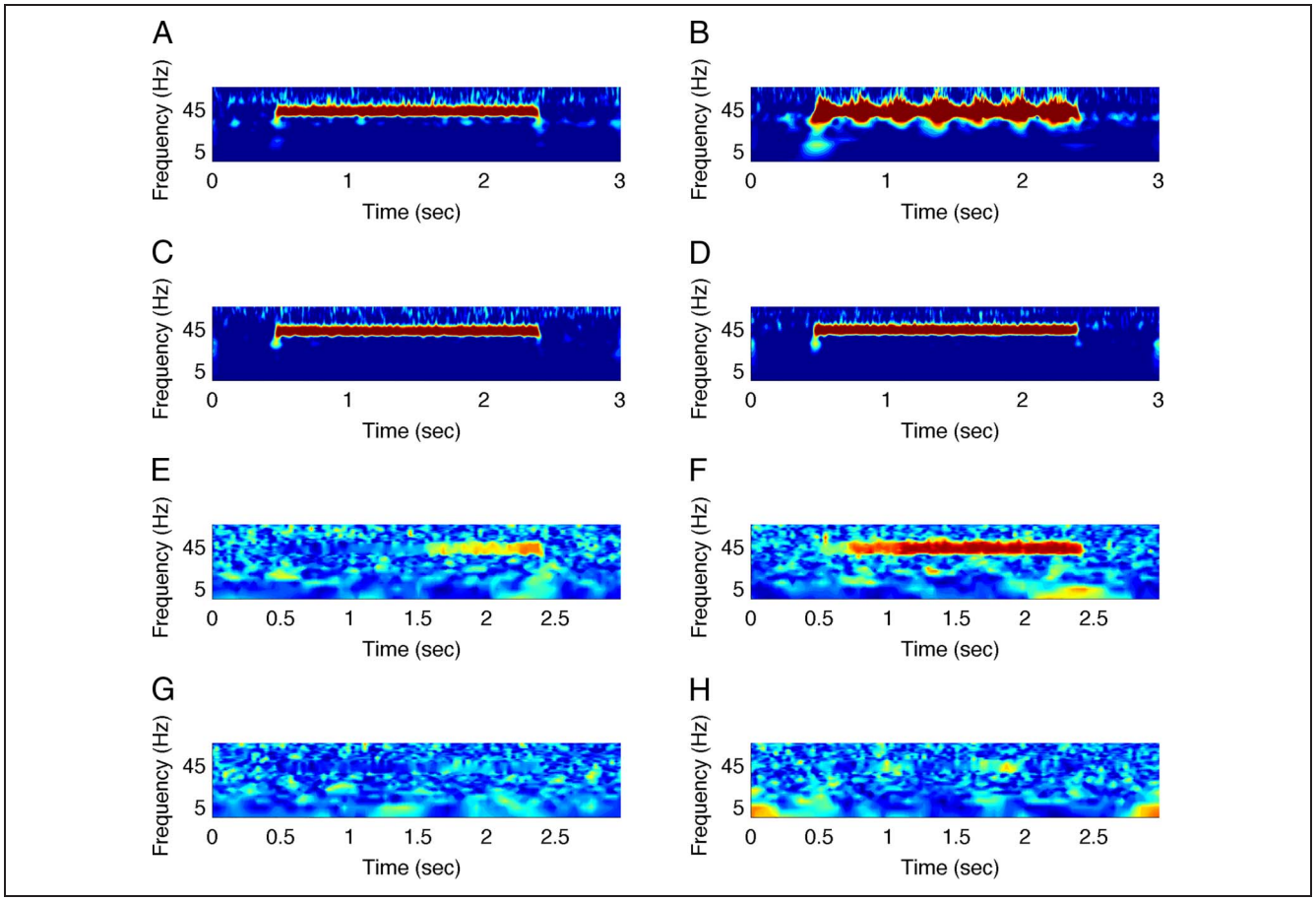

Figure 7. Time–frequency plots for representative replications in the proactive control simulation (Simulation 1). Time in a trial (in seconds) appears on the *x* axis; frequency is on the *y* axis. Stimulus onset is at 0.5 sec. Oscillation offset is at 2.5 sec. (A, B) Power in an E color neuron when $\sigma_{Pro} = 0$ and 1, respectively. (C, D) Power in an E word neuron when $\sigma_{Pro} = 0$ and 1, respectively. (E, F) Synchrony in a color–response neuron pair when $\sigma_{Pro} = 0$ and 1, respectively. (G, H) Synchrony in a word–response neuron pair when $\sigma_{Pro} = 0$ and 1, respectively.

control (Figure 7E and F, respectively). When the control signal is strong ($\sigma_{Pro} = 1$), synchrony is higher in the gamma band between these two neurons during the stimulus interval. Figure 7G–H shows the synchrony between a word neuron (same as in Figure 7C–D) and a response neuron. Although there was gamma power in this word neuron (Figure 7C–D), there is no gamma synchrony in the word–response neuron pair (Figure 7G–H).

To illustrate cross-frequency coupling, Figure 8A–B shows phase–amplitude modulation index plots for one color *E* neuron for $\sigma_{Pro} = 0$ and 1 (Figure 8A and B, respectively). Both phase and power were taken from this neuron. The phase of the slow (theta, 5 Hz) wave is locked to the power of the fast (gamma, 40 Hz) wave. Furthermore, the coupling is stronger with more power (compare Figure 8A and B). Consistently, in the literature stronger theta–gamma coupling is observed for attended stimuli, and for correct relative to error trials (Voloh et al., 2015; see Figure 3A)—presumably, stronger coupling when there is stronger control.

The time–frequency effects illustrated in Figure 7 are summarized systematically in Figure 5C–F (*nrep* = 40 per parameter value, see Methods). Although gamma power increases in both color and word neurons with increasing control (Figure 5C), gamma synchrony increases only for color–response pairs (Figure 5E). There is also increased theta power in high proactive control in MFC (Figure 5D) but limited theta synchrony (Figure 5F). Figure 8C–D summarizes the theta–gamma coupling across replications. There is limited theta–gamma coupling when phase and power were both provided by the color E neuron (Figure 8C). Instead, theta–gamma coupling was much stronger when phase was obtained from the E neuron and power from MFC (Figure 8D). Consistently, the theta–gamma modulation was strongest in empirical data (Voloh et al., 2015) when phase was taken from MFC neurons.

Simulation 2: Reactive Control

Reactive control entails that control is exerted in response to problems in ongoing processing, for example, during an experimental trial (Braver, 2012; Scherbaum, Fischer, Dshemuchadse, & Goschke, 2011). In the model, whenever response conflict (Botvinick et al., 2001) is high (typically in an incongruent trial), an extra

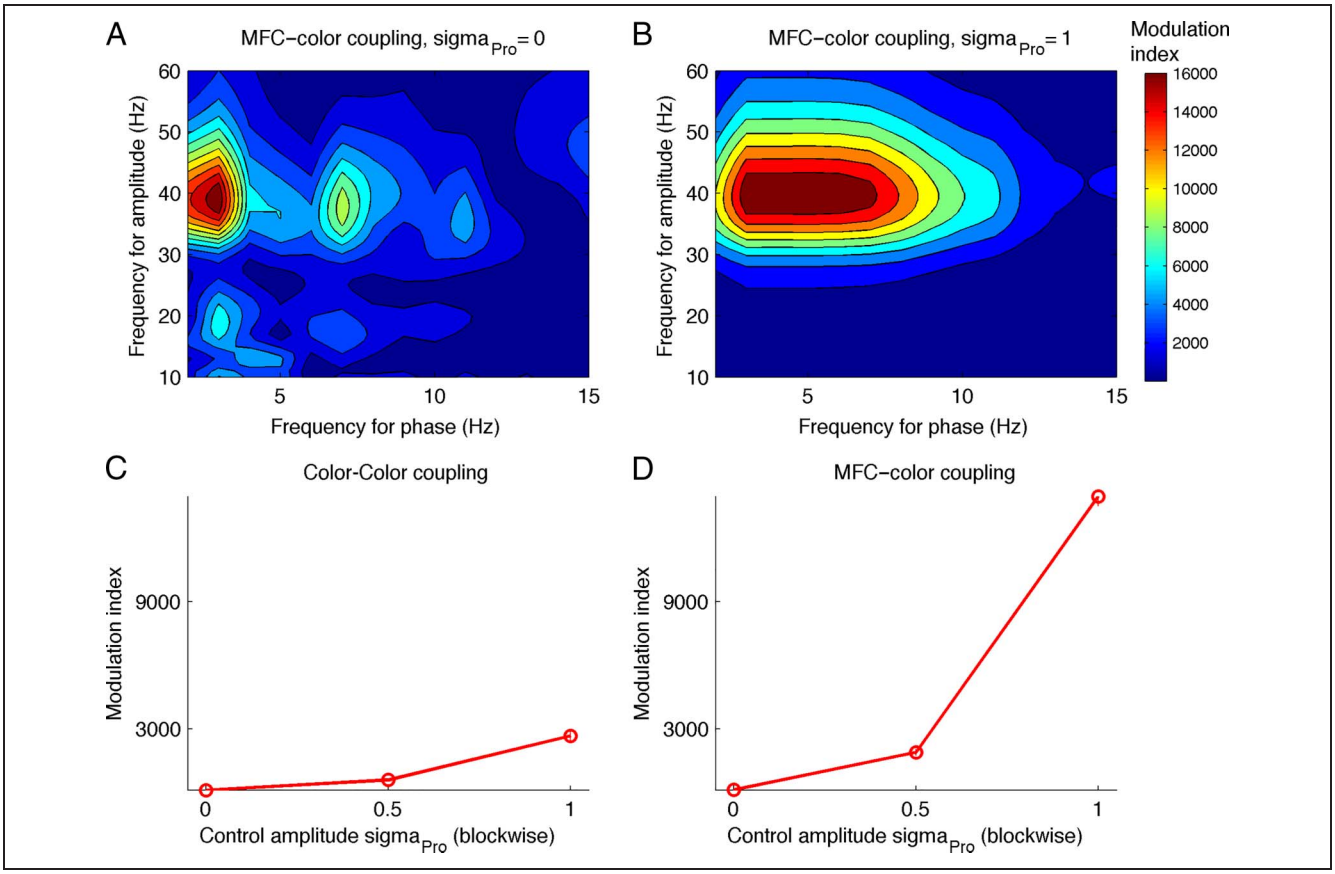

Figure 8. Cross-frequency coupling in the proactive control simulation. (A) Phase–amplitude (MFC–color) modulation in one representative $\sigma_{Pro} = 0$ replication. (B) Phase–amplitude (MFC–color) modulation in one representative $\sigma_{Pro} = 1$ replication. (C) Average phase–amplitude theta–gamma modulations when both phase and amplitude are extracted from a color *E* neuron. (D) Average phase–amplitude theta–gamma modulation when phase is extracted from MFC but amplitude from the same color *E* neuron.

reactive control (multiplicative) boost is provided to MFC phase code units. Reactive control was implemented as $\sigma_{Re} = 0$, 2, or 4. For brevity, from now on only behavioral results are plotted. Figure 9A–B shows that stronger reactive control improves performance. Note that the absolute influence of reactive control on performance is smaller than for proactive control, despite larger absolute parameter values. This is because reactive control comes "after the fact" (i.e., after stimulus processing onset) and thus cannot exert as strong an influence as proactive control.

Simulation 3: Burst Correlation

Previously, all posterior processing areas received the same MFC input, corresponding to a correlation of 1. In Figure 2A, this corresponds to the fact that the two initial (red) vectors receive the same burst. As a result, they become synchronized (Figure 2B). Suppose however that the bursts received by different areas are different; this would correspond to nonparallel kicks (dashed vectors) in Figure 2A. In this case, synchrony between areas and hence binding cannot occur. To demonstrate this property, I manipulated the correlation between color and word inputs from MFC (called burst correlation = 0, 0.5, or 1). Results appear in Figure 9C, D. The model is robust toward the assumption of equal input; even with a correlation of just 0.5, performance is better than with zero correlation. In general, performance improves with increasing correlation.

Simulation 4: Gamma Frequency Variability

Individual gamma waves must have a similar frequency; when the frequencies are too different, a continuous MFC bursting is required to keep them synchronized. To show this, I varied gamma frequency variability (σ_γ, gamma frequency variability within each single model replication *m*). Results are shown in Figure 9E, F. When σ_γ increases (and hence differences in gamma frequency between neurons and cortical areas), performance is gradually impaired.

Simulation 5: Hit Threshold

Another parameter controls at what threshold of the theta wave an MFC burst becomes possible (θ_{MFC}; see Methods). Lowering this threshold allows more MFC bursts and should thus increase control. Although the cognitive system may not control this threshold explicitly,

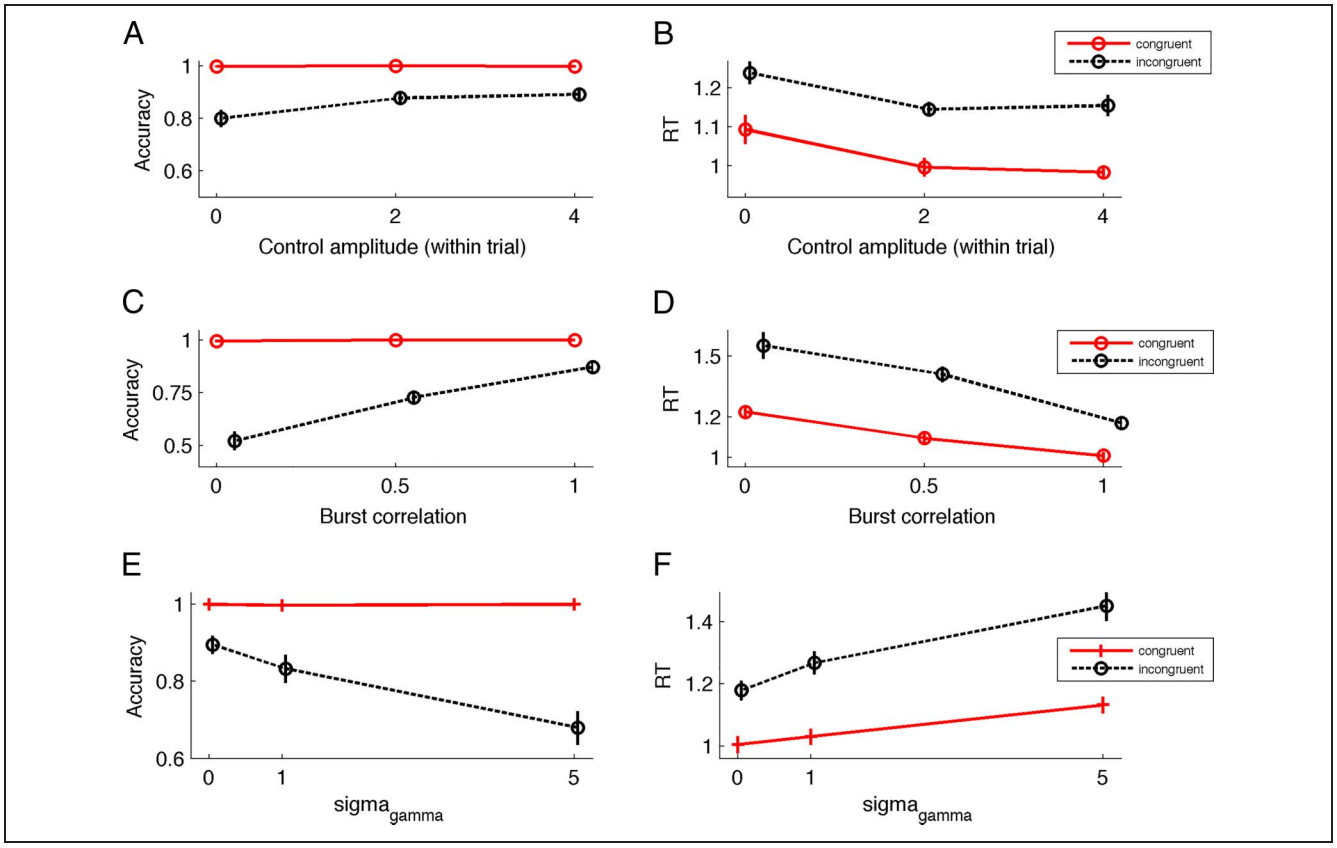

Figure 9. Behavorial results in Simulations 2–4 (σ_{Re}, burst correlation, and σ_{γ}, respectively). (A) σ_{Re} or (reactive) control amplitude within a trial. (C, D) Burst correlation. (E, F) σ_{γ} or gamma frequency standard deviation across neurons in a model replication.

I show its effect to demonstrate that lowering this threshold has the same effect as increasing theta power (see proactive and reactive control simulations). Figure 10A–B shows that this is indeed the case.

Simulation 6: Phase Threshold

The model oscillations are nonharmonic; they are effective gates that are alternatingly opened and closed for information transfer (cf. Fries, 2015). The oscillations in Figure 2B depict the nonharmonic transformations (Equation 6). The time during which the gate is opened is controlled by a parameter called phase threshold (θ_E, see Methods and Figure 2B). A higher threshold implies a shorter gate-open time, effectively decreasing the speed of information transfer between areas but also the probability of interference. Figure 10C–D shows that if the gate-open time is reduced (higher phase threshold), then RT and accuracy increase. Thus, a system may control speed–accuracy tradeoff.

Simulation 7: Response Threshold

Finally, a system may also control its speed–accuracy tradeoff by manipulating the response threshold on the response neurons (threshold θ_y). Figure 10E–F shows that this leads to similar effects as phase threshold manipulation.

DISCUSSION

A model of cognitive control based on neural synchrony between brain areas was reported. MFC and LFC collaborate to establish this synchrony. LFC establishes connections with posterior processing (e.g., color) areas, presumably during task instruction. Random bursts from MFC during task processing interact with these LFC connections. As a result, only the appropriate processing areas are synchronized, communicate more efficiently, and can implement arbitrary task rules. The model is also consistent with extant behavioral and neurophysiological data.

The model follows in a long-standing tradition of conceptualizing cognitive control as high-level actions performed by prefrontal cortex (MFC, LFC), modulating lower-level processing pathways (O'Reilly & Frank, 2006; Holroyd & Coles, 2002). In this sense, cognitive control is a higher-level form of motor control. For example, Holroyd and Coles (2002) considered MFC as a higher-level controller choosing which lower-level controller is currently allowed to guide behavior. Another line of work considered working memory as a series of abstract but learnable actions (Kriete, Noelle, Cohen, & O'Reilly, 2013;

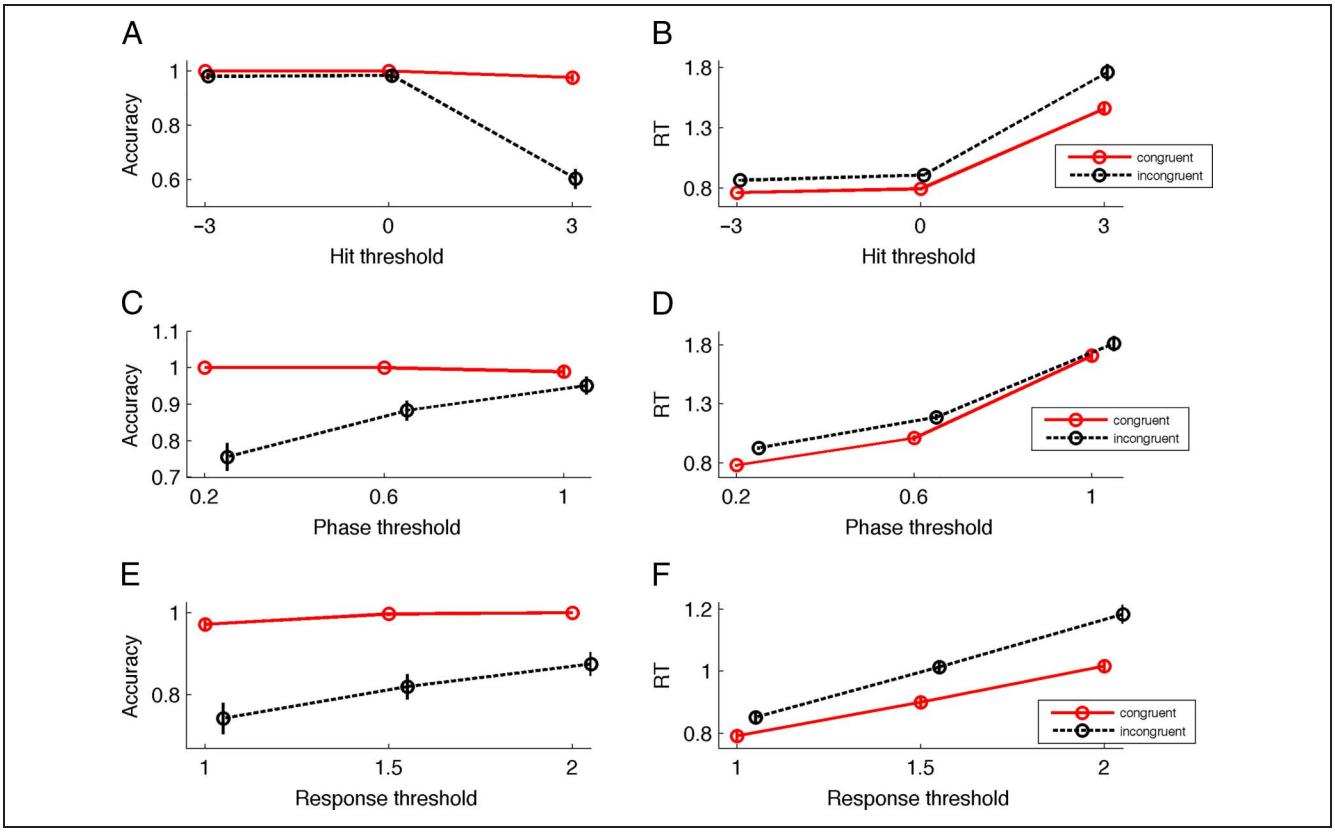

Figure 10. Behavorial results in Simulations 5–7 (thresholds θ_{MFC}, θ_E, and θ_y, respectively). (A, B) Hit threshold θ_{MFC}. (C, D) Phase threshold θ_E. (E, F) Response threshold θ_y.

O'Reilly & Frank, 2006). Also exerting effort has been modeled as a learnable action (Holroyd & McClure, 2015; Verguts, Vassena, & Silvetti, 2015; Shenhav, Botvinick, & Cohen, 2013). In the current model, synchronization between brain areas was considered to be a high-level (proactive or reactive) action.

The model was limited in some respects. First, there was no learning algorithm. Learning in oscillatory models has been rarely studied and exclusively for Hebbian learning (Li & Hertz, 2000). Powerful and feedback-based (reinforcement-based) learning rules for oscillatory models should be developed in future work. This will also allow considering the role of brainstem neuromodulators in oscillatory systems (Knowlton, Morrison, Hummel, & Holyoak, 2012). Another issue for future work is the delay between cortical areas. Although long-range communication appears possible with zero delay (Roelfsema, Engel, König, & Singer, 1997), in general brain areas may communicate with substantial delays. Efficient communication would then require a phase shift (delay) between the information-structuring oscillations (Fries, 2015). Again, from a learning perspective, the cognitive system should be able to discover which brain areas communicate with what delay and adjust its information-structuring oscillations accordingly.

Another cognitive control action that future work should consider is desynchronization. In the current model, bursts to different areas are correlated, but if bursts are negatively correlated, then areas will actually desynchronize. Empirical work has demonstrated that areas can rapidly and strongly desynchronize, suggesting that also desynchronization fulfils useful computational functions (Rodriguez et al., 1999).

The anatomical labeling was rather broad, in part because the underlying architecture is not fully known. One practical problem in human studies is that the fast timescale required for measuring frequency information is difficult to combine with high spatial resolution. However, combined EEG-fMRI studies suggest that theta frequency power in MFC for cognitive control originates from rostral cingulate zone (Debener et al., 2005). Several LFC areas have been proposed to rapidly implement task instructions. For example, inferior frontal junction locks to house- and face-sensitive areas when attending to houses and faces, respectively (Baldauf & Desimone, 2014). Also more anterior LFC areas such as dorsolateral prefrontal cortex have been implied in storing task instructions (Cole, Bagic, Kass, & Schneider, 2010; Jimura, Locke, & Braver, 2010). Furthermore, the task-specific processing areas may correspond either to isolated cortical areas (e.g., color processing) or to more distributed networks (e.g., word processing). Such areas interact with MFC and LFC (Danielmeier, Eichele, Forstmann, Tittgemeyer, & Ullsperger, 2011; Egner & Hirsch, 2005),

in specific frequency bands (Baldauf & Desimone, 2014). The response area in the processing module may correspond to premotor cortex, which strongly interacts with (other) decision-making areas (Ruge & Wolfensteller, 2012; Cisek & Kalaska, 2010). Finally, the integrator module may correspond to primary motor areas that collect evidence in favor of relevant response options (Hare, Schultz, Camerer, O'Doherty, & Rangel, 2011).

An hitherto unmentioned but relevant behavioral finding are sequential (trial-to-trial) effects; in particular, the congruency effect (in accuracy and RT) is smaller after an incongruent trial (Gratton et al., 1992). This can easily be implemented by letting theta "leak" between trials (Blais & Verguts, 2012; Scherbaum et al., 2011). Related findings such as item- and context-specific effects (Verguts & Notebaert, 2008, 2009) can similarly be addressed in future modeling with the current framework.

Why does the brain use gamma and theta waves for its cognitive bookkeeping? A number of theories have been proposed (Cohen, 2014a), but the model suggests the following intuition. First, gamma waves can embed and temporally separate the spiking of different neural populations (presumably, cognitive representations; Lisman & Jensen, 2013). Second, to understand why theta may embed gamma waves, consider Figure 1. Whereas in Figure 1A–B the gamma frequencies are the same, and in Figure 1C–D one of the gamma frequencies was slightly changed (with 2%), here, repeated theta bursts keep the gamma waves synchronized. If a theta burst is sent to the gamma-based processing modules only once, the gamma waves drift apart after soon; this happens in Figure 1E–F. The model was robust to gamma frequency perturbations (e.g., Simulation 3) because of the repeated theta bursts. However, a theta burst may also incur a cost. One reason may be that MFC projects to locus coeruleus (Aston-Jones & Cohen, 2005), whose projection to cortex may incur a cost because it leads to waste product that needs to be disposed of (Holroyd, 2016; Mather & Harley, 2016). Theta frequency may balance the costs (not too often) and benefits (sufficiently often) of binding gamma by random bursts. Finally, theta waves may be embedded in even slower (delta) waves, thus creating a hierarchy of embedded cortical frequencies. Consistently, cortical recordings reveal coupling between multi-unit activity and phase of LFPs in delta, theta, and gamma waves (Lakatos et al., 2005).

The model was inspired by a rich spectral database in perceptual and attentional processing (Gray & Singer, 1989). For example, gamma (phase) synchrony predicts the strength of coupling between cortical areas (Womelsdorf et al., 2007). Recent data additionally make a clear link to behavior. Gamma synchrony is higher for attended stimuli (Fries, Reynolds, Rorie, & Desimone, 2001); furthermore, gamma band synchrony in visual cortex predicts RT in these same data (Womelsdorf et al., 2006). Also theta power has been strongly linked to cognitive control (Cavanagh & Frank, 2014). The role of phase–amplitude (theta–gamma) coupling in cognitive control was also established recently. Theta–gamma coupling measured with intracranial EEG in human patients was increased during a broad set of cognitive tasks (Canolty et al., 2006). In a combined MFC–LFC recording study, theta–gamma coupling between MFC–LFC pairs of electrodes was recorded (Voloh et al., 2015). Consistent with the model (Figure 8), MFC provided more phase-providing LFPs than LFC. One discrepancy with these data is that the model LFC does not participate in theta–gamma binding. However, parts of the "posterior processing areas" may be represented in LFC. Furthermore, LFC circuits interact at specific (high-beta) frequencies for the implementation of cognitive tasks (Buschman et al., 2012). The exact (learning) processes in LFC remain to be studied.

Theta–gamma coupling occurs across many distal and proximal sites (e.g., hippocampus–cortex, hippocampus–striatum) and is thought to be crucial for cognitive performance. Stronger theta–gamma coupling correlates, for example, with better cognitive performance in conditional discrimination tasks in rodents (Tort et al., 2009). Furthermore, theta–gamma coupling may subserve STM (Lisman & Idiart, 1995). In particular, approximately five gamma cycles fit into one theta cycle; given that human STM consists of approximately five items, theta–gamma coupling may form its neural basis (Lisman & Jensen, 2013). The binding by random bursts principle suggests a different but not exclusive role for theta–gamma coupling; both principles exploit communication through coherence where lower-frequency waves structure faster frequency ones (Fries, 2015; Lakatos et al., 2005).

The model leads to several novel predictions. One is that the synchrony between task-relevant areas determines processing efficiency and hence accuracy and RT. In contrast, synchrony between task-irrelevant and response areas should correlate negatively with processing efficiency. This may be measured using (intracranial) EEG or MEG. Another prediction is that synchrony depends on theta power in MFC. Similar predictions can be made for (gamma) power in task-relevant brain areas. Another prediction concerns blockwise difficulty or reward manipulations in cognitive control. One can generally increase performance by making task blocks more difficult or more rewarding (Padmala & Pessoa, 2011); I predict that this effect is mediated via MFC theta. I further predict that also theta–gamma coupling between MFC and a task-relevant processing area correlates with performance. Coupling strength should be determined by MFC theta. Finally, the model predicts that spike bursts in MFC are locked to theta phase and correlated with theta power (more theta power predicts more and longer bursts).

Despite a broad variety of assumptions and implementations, models of cognitive control share a family resemblance (Alexander & Brown, 2011; Botvinick et al., 2001; Miller & Cohen, 2001). These models tend to implement learning, focus on interactions between broad anatomical areas (e.g., MFC), and address behavioral and fMRI data. For example, in Alexander and Brown (2011), the MFC

learns response–outcome conjunctions for specific stimuli and calculates prediction errors for such conjunctions. It uses these prediction errors to modulate learning of response–outcome conjunctions by a different cortical area, which itself modulates responding in posterior processing cortex. Such assumptions allow accounting for a wealth of fMRI data (also Silvetti et al., 2011). A second relevant line of modeling addresses attentional processing, and it also shares a family resemblance (Wang, 2010; Börgers, Epstein, & Kopell, 2008). Such models typically consider oscillatory interactions between areas, as implemented by biologically realistic neurons (typically, variations on the Hodgkin–Huxley conductance-based modeling system). Here, oscillations arise from pyramidal–inhibitory cell interactions, with attentional modulation from executive areas (Ardid, Wang, Gomez-Cabrero, & Compte, 2010) or from subcortical structures (Börgers et al., 2008). Such models naturally account for oscillatory interactions between cells, layers, and cortical columns. Some authors combine the strengths of these two approaches. For example, Cohen proposed that MFC cells detect simultaneous firing of motor neurons; when such (response conflict) signal is detected, MFC would broadcast this signal via theta power increases (Cohen, 2014a). As another example combining the two approaches, the current model considered how MFC and LFC cooperate using rate and phase codes to establish cognitive control.

Acknowledgments

I thank Elger Abrahamse, Peter Dayan, Wim Gevers, and Massimo Silvetti for their useful comments on this work and Peter Dayan for hosting me during his sabbatical at Gatsby Computational Neuroscience Unit (University College London). The sabbatical was supported by a travel grant from Research Foundation Flanders (V422714N) and Ghent University.

Reprint requests should be sent to Tom Verguts, Department of Experimental Psychology, Ghent University, Ghent, Belgium, or via e-mail: tom.verguts@ugent.be.

REFERENCES

Alexander, W. H., & Brown, J. W. (2011). Medial prefrontal cortex as an action-outcome predictor. *Nature Neuroscience, 14,* 1338–1344.

Ardid, S., Wang, X.-J., Gomez-Cabrero, D., & Compte, A. (2010). Reconciling coherent oscillation with modulation of irregular spiking activity in selective attention: Gamma-range synchronization between sensory and executive cortical areas. *Journal of Neuroscience, 30,* 2856–2870.

Aston-Jones, G., & Cohen, J. D. (2005). An integrative theory of locus coeruleus-norepinephrine function: Adaptive gain and optimal performance. *Annual Review of Neuroscience, 28,* 403–450.

Baldauf, D., & Desimone, R. (2014). Neural mechanisms of object-based attention. *Science, 344,* 424–427.

Blais, C., & Verguts, T. (2012). Increasing set size breaks down sequential congruency: Evidence for an associative locus of cognitive control. *Acta Psychologica, 141,* 133–139.

Börgers, C., Epstein, S., & Kopell, N. J. (2008). Gamma oscillations mediate stimulus competition and attentional selection in a cortical network model. *Proceedings of the National Academy of Sciences, U.S.A., 105,* 18023–18028.

Botvinick, M. M., Braver, T. S., Barch, D. M., Carter, C. S., & Cohen, J. D. (2001). Conflict monitoring and cognitive control. *Psychological Review, 108,* 624–652.

Braver, T. S. (2012). The variable nature of cognitive control: A dual mechanisms framework. *Trends in Cognitive Sciences, 16,* 106–113.

Braver, T. S., & Cohen, J. D. (2000). On the control of control: The role of dopamine in regulating prefrontal function and working memory. In S. Monsell & J. Driver (Eds.), *Attention & performance XVIII* (pp. 713–737). Cambridge, MA: MIT Press.

Buschman, T. J., Denovellis, E. L., Diogo, C., Bullock, D., & Miller, E. K. (2012). Synchronous oscillatory neural ensembles for rules in the prefrontal cortex. *Neuron, 76,* 838–846.

Canolty, R. T., Edwards, E., Dalal, S. S., Soltani, M., Nagarajan, S. S., Kirsch, H. E., et al. (2006). High gamma power is phase-locked to theta oscillations in human neocortex. *Science, 313,* 1626–1628.

Cavanagh, J. F., & Frank, M. J. (2014). Frontal theta as a mechanism for cognitive control. *Trends in Cognitive Sciences, 18,* 414–421.

Cisek, P., & Kalaska, J. F. (2010). Neural mechanisms for interacting with a world full of action choices. *Annual Review of Neuroscience, 33,* 269–298.

Cohen, J. D., Dunbar, K., & McClelland, J. L. (1990). On the control of automatic processes: A parallel distributed processing account of the Stroop effect. *Psychological Review, 97,* 332–361.

Cohen, M. X. (2014a). A neural microcircuit for cognitive conflict detection and signaling. *Trends in Neurosciences, 37,* 480–490.

Cohen, M. X. (2014b). *Analyzing neural time series data*. Cambridge, MA: MIT Press.

Cole, M. W., Bagic, A., Kass, R., & Schneider, W. (2010). Prefrontal dynamics underlying rapid instructed task learning reverse with practice. *Journal of Neuroscience, 30,* 14245–14254.

Danielmeier, C., Eichele, T., Forstmann, B. U., Tittgemeyer, M., & Ullsperger, M. (2011). Posterior medial frontal cortex activity predicts post-error adaptations in task-related visual and motor areas. *Journal of Neuroscience, 31,* 1780–1789.

Debener, S., Ullsperger, M., Siegel, M., Fiehler, K., von Cramon, D. Y., & Engel, A. K. (2005). Trial-by-trial coupling of concurrent electroencephalogram and functional magnetic resonance imaging identifies the dynamics of performance monitoring. *Journal of Neuroscience, 25,* 11730–11737.

Desimone, R., & Duncan, J. (1995). Neural mechanisms of visual selective attention. *Annual Review of Neuroscience, 18,* 193–222.

Doll, B. B., Jacobs, W. J., Sanfey, A. G., & Frank, M. J. (2009). Instructional control of reinforcement learning: A behavioral and neurocomputational investigation. *Brain Research, 1299,* 74–94.

Douglas, R. J., Martin, K. A. C., & Whitteridge, D. (1989). A canonical microcircuit for neocortex. *Neural Computation, 1,* 480–488.

Egner, T., & Hirsch, J. (2005). Cognitive control mechanisms resolve conflict through cortical amplification of task-relevant information. *Nature Neuroscience, 8,* 1784–1790.

Engel, A. K., Fries, P., & Singer, W. (2001). Dynamic predictions: Oscillations and synchrony in top–down processing. *Nature Reviews Neuroscience, 2,* 704–716.

Fell, J., & Axmacher, N. (2011). The role of phase synchronization in memory processes. *Nature Reviews Neuroscience, 12,* 105–118.
Fries, P. (2009). Neuronal gamma-band synchronization as a fundamental process in cortical computation. *Annual Review of Neuroscience, 32,* 209–224.
Fries, P. (2015). Rhythms for cognition: Communication through coherence. *Neuron, 88,* 220–235.
Fries, P., Reynolds, J. H., Rorie, A. E., & Desimone, R. (2001). Modulation of oscillatory neuronal synchronization by selective visual attention. *Science, 291,* 1560–1563.
Giraud, A.-L., & Poeppel, D. (2012). Cortical oscillations and speech processing: Emerging computational principles and operations. *Nature Neuroscience, 15,* 511–517.
Gratton, G., Coles, M. G. H., & Donchin, E. (1992). Optimizing the use of information: Strategic control of activation of responses. *Journal of Experimental Psychology. General, 121,* 480–506.
Gray, C. M., König, P., Engel, A. K., & Singer, W. (1989). Oscillatory responses in cat visual cortex exhibit inter-columnar synchronization which reflects global stimulus properties. *Nature, 338,* 334–337.
Gray, C. M., & Singer, W. (1989). Stimulus-specific neuronal oscillations in orientation columns of cat visual cortex. *Proceedings of the National Academy of Sciences, U.S.A., 86,* 1698–1702.
Hare, T. A., Schultz, W., Camerer, C. F., O'Doherty, J. P., & Rangel, A. (2011). Transformation of stimulus value signals into motor commands during simple choice. *Proceedings of the National Academy of Sciences, U.S.A., 108,* 18120–18125.
Holroyd, C. B. (2016). The waste disposal problem of effortful control. In T. S. Braver (Ed.), *Motivation and cognitive control* (pp. 235–260). Hove, UK: Psychology Press.
Holroyd, C. B., & Coles, M. G. H. (2002). The neural basis of human error processing: Reinforcement learning, dopamine, and the error-related negativity. *Psychological Review, 109,* 679–709.
Holroyd, C. B., & McClure, S. M. (2015). Hierarchical control over effortful behavior by rodent medial frontal cortex: A computational model. *Psychological Review, 122,* 54–83.
Huang, T., Hazy, T. E., Herd, S. A., & O'Reilly, R. C. (2013). Assembling old tricks for new tasks: A neural model of instructional learning and control. *Journal of Cognitive Neuroscience, 25,* 843–851.
Hummel, J. E., & Biederman, I. (1992). Dynamic binding in a neural network for shape recognition. *Psychological Review, 99,* 480–517.
Hummel, J. E., & Holyoak, K. J. (2003). A symbolic-connectionist theory of relational inference and generalization. *Psychological Review, 110,* 220–264.
Janssens, C., De Loof, E., Pourtois, G., & Verguts, T. (2016). The time course of cognitive control implementation. *Psychonomic Bulletin & Review, 23,* 1266–1272.
Jensen, O., Bonnefond, M., & VanRullen, R. (2012). An oscillatory mechanism for prioritizing salient unattended stimuli. *Trends in Cognitive Sciences, 16,* 200–206.
Jimura, K., Locke, H. S., & Braver, T. S. (2010). Prefrontal cortex mediation of cognitive enhancement in rewarding motivational contexts. *Proceedings of the National Academy of Sciences, U.S.A., 107,* 8871–8876.
Knowlton, B. J., Morrison, R. G., Hummel, J. E., & Holyoak, K. J. (2012). A neurocomputational system for relational reasoning. *Trends in Cognitive Sciences, 16,* 373–381.
Kriete, T., Noelle, D. C., Cohen, J. D., & O'Reilly, R. C. (2013). Indirection and symbol-like processing in the prefrontal cortex and basal ganglia. *Proceedings of the National Academy of Sciences, U.S.A., 110,* 16390–16395.
Lachaux, J.-P., Rodriguez, E., Martinerie, J., & Varela, F. J. (1999). Measuring phase synchrony in brain signals. *Human Brain Mapping, 8,* 194–208.
Lakatos, P., O'Connell, M. N., Barczak, A., Mills, A., Javitt, D. C., & Schroeder, C. E. (2009). The leading sense: Supramodal control of neurophysiological context by attention. *Neuron, 64,* 419–430.
Lakatos, P., Shah, A. S., Knuth, K. H., Ulbert, I., Karmos, G., & Schroeder, C. E. (2005). An oscillatory hierarchy controlling neuronal excitability and stimulus processing in the auditory cortex. *Journal of Neurophysiology, 94,* 1904–1911.
Li, Z., & Hertz, J. (2000). Odour recognition and segmentation by a model olfactory bulb and cortex. *Network: Computation in Neural Systems, 11,* 83–102.
Li, Z., & Hopfield, J. J. (1989). Modeling the olfactory bulb and its neural oscillatory processings. *Biological Cybernetics, 61,* 379–392.
Lisman, J. E., & Idiart, M. A. (1995). Storage of 7 plus / minus 2 short-term memories in oscillatory subcycles. *Science, 267,* 1512–1515.
Lisman, J. E., & Jensen, O. (2013). The θ-γ neural code. *Neuron, 77,* 1002–1016.
Loftus, G. R., & Masson, M. E. J. (1994). Using confidence intervals in within-subject designs. *Psychonomic Bulletin & Review, 1,* 476–490.
Mather, M., & Harley, C. W. (2016). The locus coeruleus: Essential for maintaining cognitive function and the aging brain. *Trends in Cognitive Sciences, 20,* 214–226.
Miller, E. K., & Cohen, J. D. (2001). An integrative theory of prefrontal cortex function. *Annual Review of Neuroscience, 24,* 167–202.
Miltner, W. H. R., Braun, C., Arnold, M., Witte, H., & Taub, E. (1999). Coherence of gamma-band EEG activity as a basis for associative learning. *Nature, 397,* 434–436.
Nakao, H., Arai, K. S., Nagai, K., Tsubo, Y., & Kuramoto, Y. (2005). Synchrony of limit-cycle oscillators induced by random external impulses. *Physical Review E-Statistical, Nonlinear, and Soft Matter Physics, 72,* 1–13.
Nigbur, R., Cohen, M. X., Ridderinkhof, K. R., & Stürmer, B. (2012). Theta dynamics reveal domain-specific control over stimulus and response conflict. *Journal of Cognitive Neuroscience, 24,* 1264–1274.
Onslow, A. C. E., Jones, M. W., & Bogacz, R. (2014). A canonical circuit for generating phase–amplitude coupling. *PLoS One, 9,* e102591.
O'Reilly, R. C., & Frank, M. J. (2006). Making working memory work: A computational model of learning in the prefrontal cortex and basal ganglia. *Neural Computation, 18,* 283–328.
Padmala, S., & Pessoa, L. (2011). Reward reduces conflict by enhancing attentional control and biasing visual cortical processing. *Journal of Cognitive Neuroscience, 23,* 3419–3432.
Pastötter, B., Dreisbach, G., & Bäuml, K. T. (2013). Dynamic adjustments of cognitive control: Oscillatory correlates of the conflict adaptation effect. *Journal of Cognitive Neuroscience, 25,* 2167–2178.
Ramamoorthy, A., & Verguts, T. (2012). Word and deed: A computational model of instruction following. *Brain Research, 1439,* 54–65.
Rodriguez, E., George, N., Lachaux, J., Martinerie, J., Renault, B., & Varela, F. J. (1999). Perception's shadow: Long-distance synchronization of human brain activity. *Nature, 397,* 430–433.
Roelfsema, P. R., Engel, A. K., König, P., & Singer, W. (1997). Visuomotor integration is associated with zero time-lag synchronization among cortical areas. *Nature, 385,* 157–161.
Ruge, H., & Wolfensteller, U. (2012). Functional integration processes underlying the instruction-based learning of novel goal-directed behaviors. *Neuroimage, 68,* 162–172.

Scherbaum, S., Fischer, R., Dshemuchadse, M., & Goschke, T. (2011). The dynamics of cognitive control: Evidence for within-trial conflict adaptation from frequency-tagged EEG. *Psychophysiology, 48,* 591–600.
Schroeder, C. E., & Lakatos, P. (2009). Low-frequency neuronal oscillations as instruments of sensory selection. *Trends in Neurosciences, 32,* 9–18.
Shenhav, A., Botvinick, M. M., & Cohen, J. D. (2013). The expected value of control: An integrative theory of anterior cingulate cortex function. *Neuron, 79,* 217–240.
Silvetti, M., Seurinck, R., & Verguts, T. (2011). Value and prediction error in medial frontal cortex: Integrating the single-unit and systems levels of analysis. *Frontiers in Human Neuroscience, 5,* 75.
Tort, A. B. L., Komorowski, R. W., Manns, J. R., Kopell, N. J., & Eichenbaum, H. (2009). Theta–gamma coupling increases during the learning of item-context associations. *Proceedings of the National Academy of Sciences, U.S.A., 106,* 20942–20947.
Usher, M., & McClelland, J. L. (2001). The time course of perceptual choice: The leaky, competing accumulator model. *Psychological Review, 108,* 550–592.
Vassena, E., Silvetti, M., Boehler, C. N., Achten, E., Fias, W., & Verguts, T. (2014). Overlapping neural systems represent cognitive effort and reward anticipation. *PLoS One, 9,* 1–9.
Verguts, T., & Notebaert, W. (2008). Hebbian learning of cognitive control: Dealing with specific and nonspecific adaptation. *Psychological Review, 115,* 518–525.
Verguts, T., & Notebaert, W. (2009). Adaptation by binding: A learning account of cognitive control. *Trends in Cognitive Sciences, 13,* 252–257.
Verguts, T., Vassena, E., & Silvetti, M. (2015). Adaptive effort investment in cognitive and physical tasks: A neurocomputational model. *Frontiers in Behavioral Neuroscience, 9,* 1–17.
Voloh, B., Valiante, T. A., Everling, S., & Womelsdorf, T. (2015). Theta–gamma coordination between anterior cingulate and prefrontal cortex indexes correct attention shifts. *Proceedings of the National Academy of Sciences, U.S.A., 112,* 201500438.
Wang, X.-J. (2010). Neurophysiological and computational principles of cortical rhythms in cognition. *Physiological Reviews, 90,* 1195–1268.
Womelsdorf, T., Fries, P., Mitra, P. P., & Desimone, R. (2006). Gamma-band synchronization in visual cortex predicts speed of change detection. *Nature, 439,* 733–736.
Womelsdorf, T., Johnston, K., Vinck, M., & Everling, S. (2010). Theta-activity in anterior cingulate cortex predicts task rules and their adjustments following errors. *Proceedings of the National Academy of Sciences, U.S.A., 107,* 5248–5253.
Womelsdorf, T., Schoffelen, J.-M., Oostenveld, R., Singer, W., Desimone, R., Engel, A. K., et al. (2007). Modulation of neuronal interactions through neuronal synchronization. *Science, 316,* 1609–1612.
Wong, K.-F., & Wang, X.-J. (2006). A recurrent network mechanism of time integration in perceptual decisions. *Journal of Neuroscience, 26,* 1314–1328.
Zhou, T., Chen, L., & Aihara, K. (2005). Molecular communication through stochastic synchronization induced by extracellular fluctuations. *Physical Review Letters, 95,* 2–5.